Rheinisch-Westfälische Technische Hochschule Aachen
Institut für Bildsame Formgebung

Generation of open-die forging FE-models and integration of a microstructure material model

Hauptseminar

Paul Hibbe, B. Sc. RWTH
Matthias Nick, B. Sc. RWTH

Durchgeführt in der Abteilung Werkstoffmodellierung
im WS 2013/14

Betreuer: Univ. Prof. Dr.-Ing. Gerhard Hirt
Dipl.-Ing. Thomas Henke
Stephan Hojda, M. Sc. RWTH

Contents

1 Introduction

Open-die forging is the oldest forging process and can be used to create a variety of final forms. It is an incremental, highly flexible metal forming process. The process typically involves two dies of simple geometry moving towards one another and thus forming the work piece. Open-die forging processes can be separated into four categories: upsetting, stretch forging, punching and hollow forging. This work, however, will focus on a stretch forging process.[DB07]

Since the properties of the work piece depend strongly on the microstructure, methods to predict microstructural behaviour have been researched. The calculation of microstructure devolution based on the Finite Element modelling of the macroscopic mechanical process has proven to produce good results in this field. However, a systematic approach to test these results for open-die forging processes has yet to be undertaken. This work will focus on the microstructural modelling of a process that can easily be reproduced in reality.

Besides, the Finite Element results of the primarily used FEM package will be validated using other software. Software packages will be compared based on their usability and flexibility to describe open-die forging processes.

2 Fundamentals

2.1 Open-die forging

The incremental and flexible nature of open-die forging makes it suitable primarily to the manufacturing of small lot sizes or for the forming of parts that cannot be produced by other processes due to power and force limitations of these processes. Its primary use is in the preparation of cast ingots for further machining. By open-die forging, cavities from the casting process can be rectified and the needed material properties can be reached.[DHK+11]

2.2 Finite element method

The finite element method is a method to model, beside others, continuum mechanics of solid work pieces. The work piece is separated into discrete parts, called elements, which are themselves geometrically defined by nodes. While these nodes hold coordinates as information, the elements hold temperatures, stresses etc. Using material properties such as flow curves, friction, thermal conductivity and emissivity, the system's reaction to thermal and mechanical external loads can be calculated.

Due to the non-linear nature of the resulting equation system, only very simple models can be calculated analytically while most must be approximated numerically. Besides matters of usability, the numerical approach is the most important difference between available software packages. These are spread across a wide spectrum from academic systems with large freedom for the user to easy-to-use specialized tools for certain uses.

3 Model process

This work deals with modeling of an open die forging process with multiple passes. The material used is a common stainless steel. The process parameters are orientated on a plan for forging a block with four passes given by the forging simulation software ForgeBase. Important process parameters, besides the flow curves, are for example the material data, the height reduction during every pass, the movement of the die, meaning the kinematics, the process temperature, etc. The detailed process conditions are discussed in the following chapters.

3.1 Material data

The material used is a 1.4301 (X5CrNiMo18-10) stainless steel. It is an austenitic steel which contains high quantities of the alloying elements chrome and nickel 3.1. Therefore it is non-corrosive, acid- and heat-resistant. The field of application is widely spread and reaches from the automotive industry up to the chemical industry [Ede08].

The chemical composition (in weight-%) of the material is as follows [met14]:

Table 3.1: Chemical composition of 1.4301

C[%]	Cr[%]	Ni[%]	Si[%]	Mn[%]	P[%]	S[%]	N[%]
max 0,07	17,00-19,50	8,00-10,50	max 1,00	max. 2,00	max 0,045	max 0,03	max 0,11

For the input in a simulation model the thermal material data is crucial, containing are the temperature depending thermal conductivity, the spec. heat capacity and the Young´s modul, see figure 3.1, 3.2, 3.3.

It is necessary that the data describes the whole temperature range of the process. Further parameters are set constant and are pictured in 3.2.

Table 3.2: Constant process parameters (reference temperature 20°C)

Poison	0,3	-
Thermal expansion	0,000012	[1/K]
Emissivity	0,7	-
Heat transfer coeff.	4,5	[W/(m²K)]
Friction coeff.	0,4	-
Dissipation	0,9	%

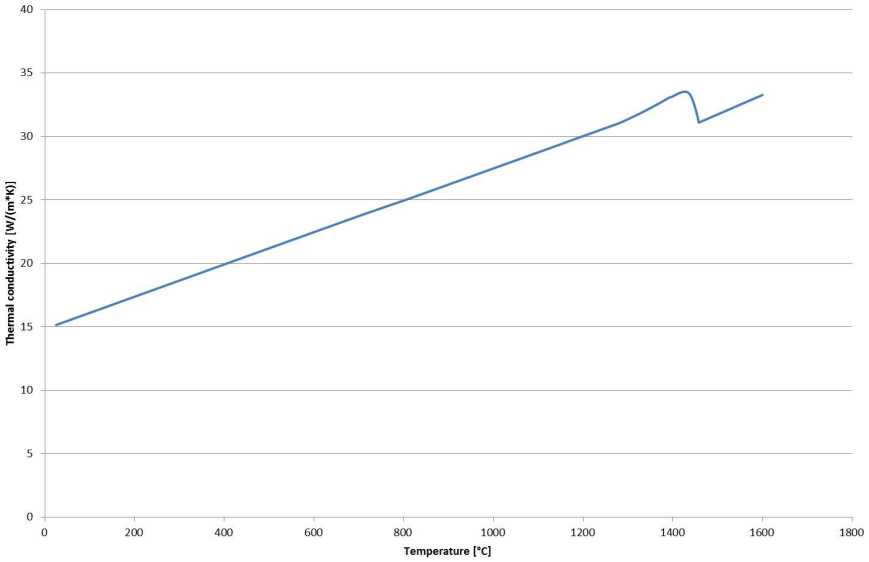

Figure 3.1: Thermal conductivity of 1.4301

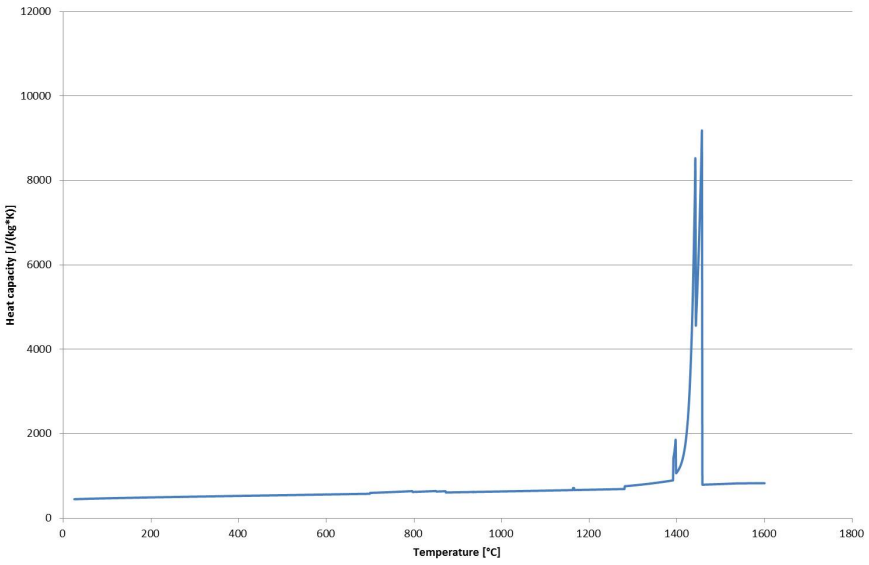

Figure 3.2: Heat capacity of 1.4301

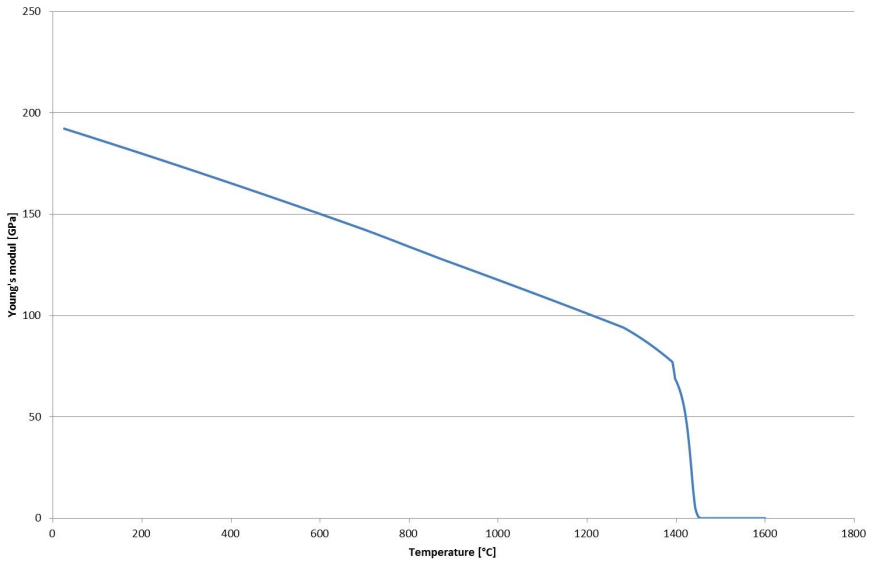

Figure 3.3: Young's modul of 1.4301

3.2 Forging plan (ForgeBase)

The settings of the forging simulation are based on the calculation of the forging software ForgeBase 3.3. The simulations are done for a four passes process on a block (workpiece - WP) with the dimensions of 150mm in height as well as in width and 600mm in length. However, only 400mm of the length are forged. The rest is provided for the manipulator to hold and move the WP. The WP is set as a plastic solid and is meshed with a brick mesh with 12544 elements. The upper and lower dies are set as rigid object. The manipulator is set up as a spring with a stiffness of 175 N/mm and the maximum clamping force of 222,4 kN.

The passes in the simulation vary in height reduction and bite ratio. Between the passes the WP is rotated in positive and negative direction with 90° rotation angle. There are two models of movement. On the one hand the bottom die is fixed, though the top die moves with a speed of 80mm/s (Simufact). On the other hand the top and the bottom die move with a speed of 40mm/s (DEFORM; PEP/LARSTRAN).

Moreover, the heat treatment before and during the process is of great importance. Before the first pass starts, the WP gets heated up to 1200°C for 2 hours. It is vital, that the WP does have a homogeneous distribution. During the forging passes, heat is getting lost by the effects of emission and the heat transfers to the dies. Because of that,

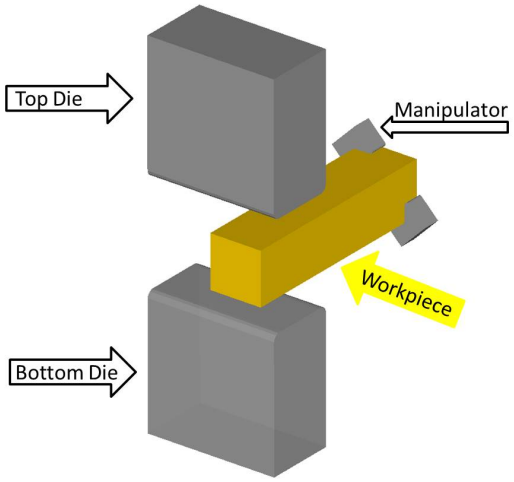

Figure 3.4: Illustration of the process setup from DEFORM

Table 3.3: Forging plan from ForgeBase

Pass Nr.	Reduction [mm]	Height 1 [mm]	Width 1 [mm]	Height 2 [mm]	Width 2 [mm]	Rotation [°]	Bite width [mm]
0	0	150	150	150	150	0	0
1	28	122	162	122	162	0	105
2	30	132	132	132	132	90	85
3	25	107	143	107	143	-90	92
4	27	116	116	116	116	90	75

a second heat is necessary between the second and the third pass. The WP is heated up again to 1200°C within 1 hour. After the last pass the WP cools down upon air to room temperature.

4 Material modeling

This chapter deals with the concept of material modeling based on semi-empirical equations. At first there will be a short overview of the mechanisms of recovery and recrystallization and after that a review of common models describing the evolution of microstructure during hot forming and a way to integrate them into common FEM-software.

4.1 Recovery and recrystallization

The flow stress is highly dependent on microstructural softening and hardening mechanism during forming. In addition, these mechanisms are influenced by the temperature, strain rate and strain.

During hot forming, defects are generated within the crystal lattice. According to Gottstein [Got07] the defects can be distinguished respecting their dimensions. Especially one dimensional defects called dislocations, are the carriers of plastic deformation and therefore crucial for hot working. During hot deformation the density of dislocations rises and hence the resistance of the material to deformation rises too. At a certain point the stored energy in the material is high enough to induce dynamic recovery (DRV) or dynamic recrystallization (DRX). These mechanisms cause softening of the material.

DRV leads to equilibrium between hardening and softening. However DRX leads to a softened material. The effects of DRV and DRX can be well seen in the warm flow curve behavior, see 4.1.

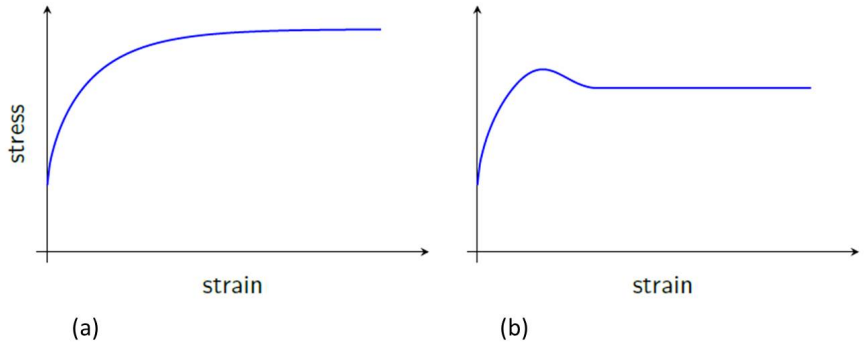

Figure 4.1: Warm flow curves when recovery (a) or recrystallization (b) is predominant [Loh10]

The softening effect of DRV and therefore the reduced level of stress with increasing strain is based on the rearrangement and annihilation of dislocations [Gottstein]. During DRX new grains are built and grow at spots with low specific energy. Both effects lead to a totally refined microstructure.

After hot forming, remaining dislocations can still store a great amount of energy. This energy can be enough to cause static recovery (SRV) or static recrystallization (SRX). These processes take place during heat treatment after warm forming. The softening effects are the same as in DRV or DRX. The driving force drops during SRV and SRX and only when there is enough energy stored, SRV and SRX lead to a fully refined microstructure.

After or parallel to SRV and SRX, grain growth (GG) can take place. The driving force is the reduction of stored energy. During grain growth the nucleated grains grow by using up the old grain structure.

4.2 gives a short summary about the recovery, recrystallization and grain growth mechanisms during warm forming.

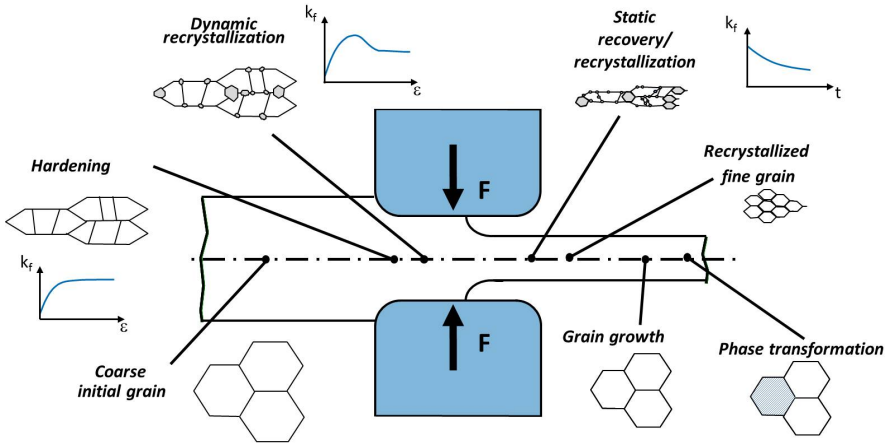

Figure 4.2: Recovery and recrystallization mechanisms during warm forming

The flow curves 4.3 are essential for the determination of the recrystallization kinetics and the fraction of recrystallized material. Therefore it is the basis for the creation of a microstructure model. At the IBF, flow curves are determined by isothermal compression tests at cylindrical specimens with an eight to diameter ratio of 1,5. For the 1.4301 tests have been carried out at temperatures ranging from $900 - 1250°C$ and strain rates of $0,05 - 100s^{-1}$ 4.3.

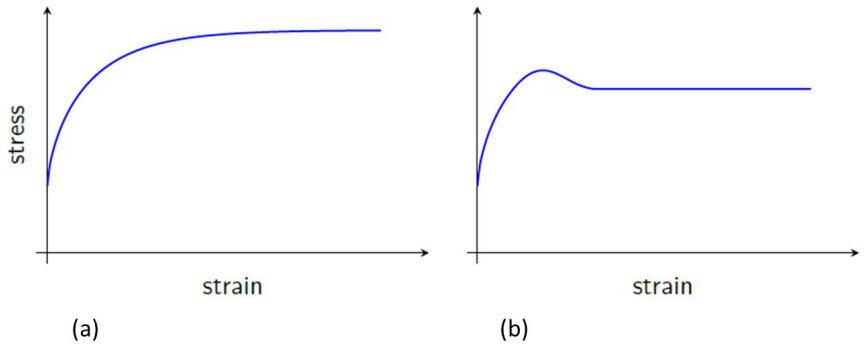

Figure 4.3: Determined flow curves of 1.4301 (temperature range: 900-1250°C)

For the semi empirical material model given by Deghan Manshadi [ARP08] the special strain values are of great importance. These strain states are seen in 4.4. There is the peak strain ε_p, the strain of steady state ε_{ss}, and not seen in 4.4 the critical strain ε_c which is located at 60% of the peak strain. The stresses at these characteristic points are also of importance.

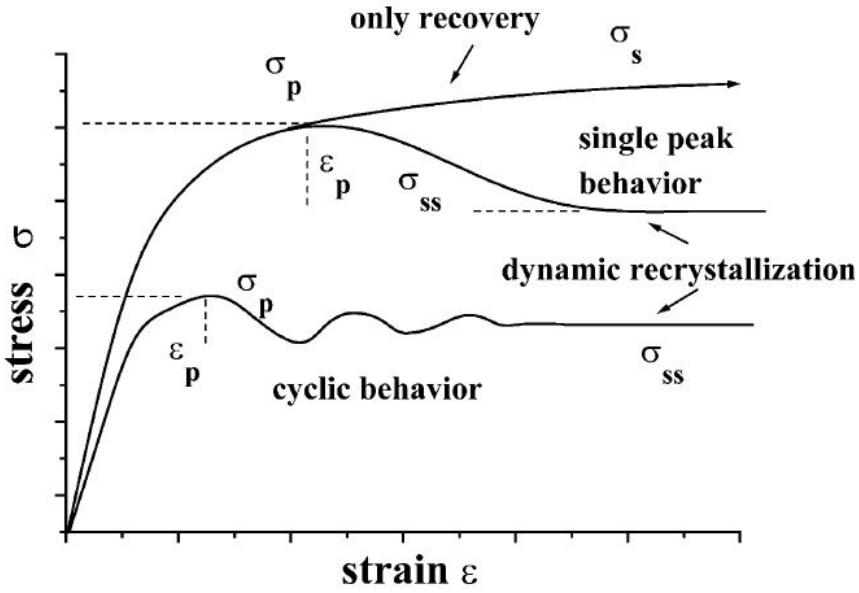

Figure 4.4: Warm flow curves with characteristic stress and strain points [MJJ03]

They can also be calculated by:

$$\varepsilon_p = 3,6 \cdot 10^{-3} d_0^0 \cdot Z^{0,15} \tag{4.1}$$

$$\varepsilon_c = 0,6 \cdot \varepsilon_p \tag{4.2}$$

$$\varepsilon_{ss} = 0,00598 \cdot d_0^0 \cdot Z^{0,1536} \tag{4.3}$$

4.2 Semi emprirical material models

For the prediction of microstructural evolution semi-empirical models are used for many years. Lohmar and Karhausen gave a detailed overlook over the common models used in warm forming [Loh10][Kar94].

The JMAK-equation is a way to calculate the fraction of recrystallization X 4.5 for the different recrystallization mechanisms DRX and SRX. In this work the equation for the calculation of DRX and SRX published by Dehgan Manshadi is used [ARP08].

$$X = 1 - exp\left(log\left(1 - 0,95\right) \cdot \left(\frac{\varepsilon_{eff} - \varepsilon_c}{\varepsilon_x}\right)^{1,3}\right) \tag{4.4}$$

$$X = 1 - exp\left(log\left(1 - 0,5\right) \cdot \left(\frac{t_{SRX}}{t_{50}}\right)^{1,1}\right) \tag{4.5}$$

Where t_{50} is the time where 50% recrystallization took place 4.5:

$$t_{50} = 8 \cdot 10^{-9} \varepsilon^{-1,5} \cdot Z^{-0,42} exp\left(\frac{375000}{R \cdot T}\right) \tag{4.6}$$

A lot of these models relate the stress behavior to the strain rate $\dot{\varepsilon}$ and the Temperature T. A popular way to describe this is given by the Zener-Hollomon parameter Z [CH44]:

$$Z = \varepsilon \cdot exp\left(\frac{Q}{R \cdot T}\right) \tag{4.7}$$

These equations lead to the determination of the grain size d_{DRX} and d_{SRX} [ARP08]:

$$d_{DRX} = 5916 \cdot Z^{-0,1748} \tag{4.8}$$

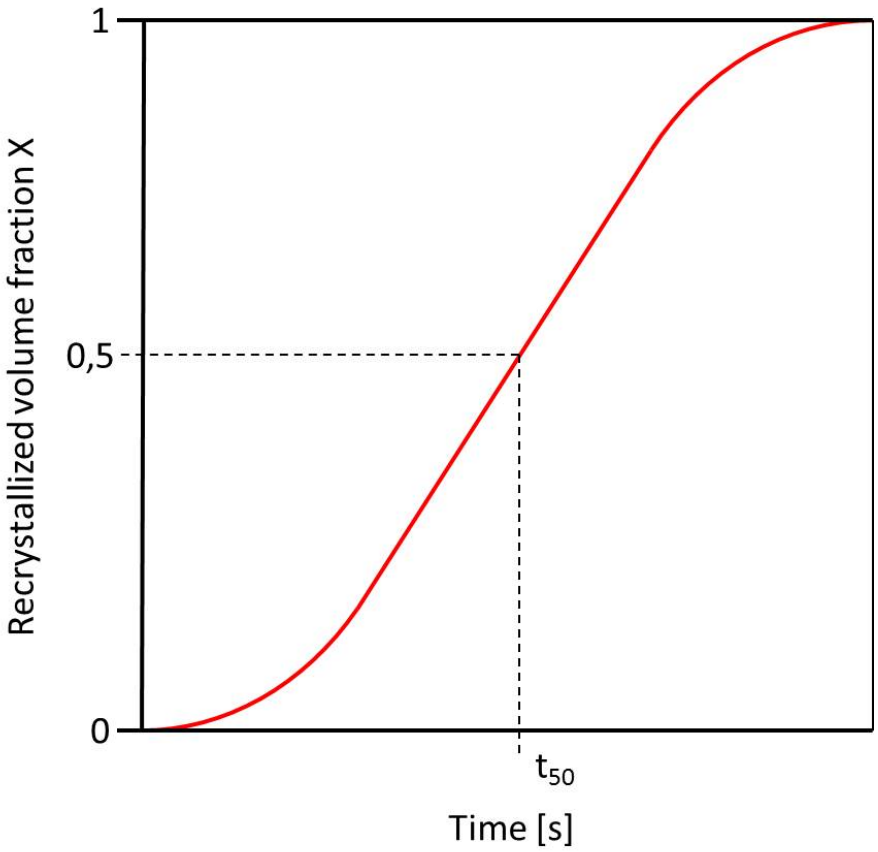

Figure 4.5: Fraction of recrysrallization X

$$d_{SRX} = 4,7 \cdot 10^2 \cdot \varphi_{SRX^{-1}} \cdot 100^{0,3} \cdot Z^{-0,1} \tag{4.9}$$

5 Validation

For the modelling of the described process, different software packages are available. Besides DEFORM3D, both FORGE from Transvalor, Mougins, France, and a combination of PEP (Pre- and Postprocessing Environment for Programmers) developed at IBF and LARSTRAN from LASSO Ingenieurgesellschaft mbH, Leinfelden, Germany have been used to validate the results. The packages differ in their ease of use and freedom in modelling. A comparison of both usability and results will be made here.

5.1 DEFORM

Based on the finite element method DEFORM is a tool for the prediction of material flow and thermal behavior in forming processes. Several deformation modes are given by the software package (forging, rolling, extrusion, upsetting, cogging, etc.). The system provides different material models (rigid, plastic, rigid-plastic), forming equipment (hydraulic presses, hammers, screw presses) and the possibility of setting individual boundary conditions (friction, thermal). The DEFORM postprocessor offers the option of contour plots, stroke prediction, point tracking and other features [DEF14]. In this work the Cogging deformation mode is used. For the process conditions see chapter 3.

5.1.1 Forging Forces

One of the essential values in cogging operation is the forging force. The forging force is vital to predict the press limits and therefore for the process dimensioning. The forging force is extracted in the postprocessor in form of a process time against die force plot. The graphs show the increasing force during the four passes. The number of bites does vary from pass to pass depending on the bite width. It starts with four bites in the first pass and eight bites in the last one (figures 5.1 and 5.2). The maximum die force is about 3150kN and the minimum force is about 1680kN. The differential of these values can be explained of the variety in the pressed surface. Especially in the last stroke not all of the bite length is presses because the 200mm for the manipulator to grab the WP is not forged. The oscillation of the die force can be explained by the forging history of the presses material. The material is not totally homogeneously forged. This effect will be explained later. However in average the die force is about the magnitude which can be calculated roughly by Siebel, $F = 2.5\text{MN}$:

$$F = s_b \cdot b \cdot 1.15 \cdot k_f \left(1 + \frac{\mu \cdot s_b}{2 \cdot h} + \frac{h}{h \cdot s_b}\right) \tag{5.1}$$

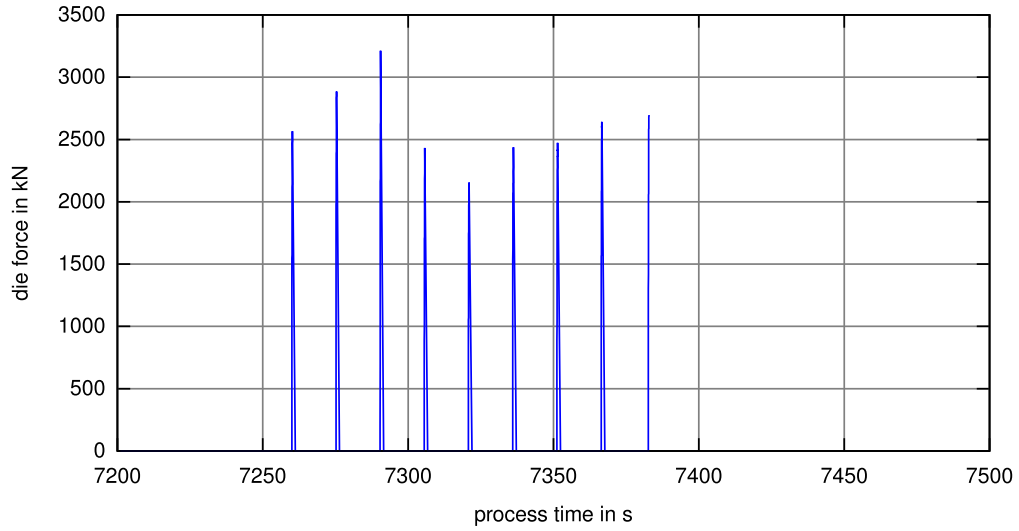

Figure 5.1: Forging forces for passes 1 and 2 as calculated by DEFORM3D

The characteristic of the die force during a bite (figure 5.3) is that the die force increases because of strain hardening and area increase with forming stroke up to a maximum. The inconsistent in the die force increasing can be explained by the die instantly getting more contact nodes and therefore an increasing surface to press. The linear force drop after the maximum is affected by the used time step. Normally the die force should drop to zero immediately.

5.1.2 Strain

The aim for a well forged ingot is a homogeneous strain distribution in the core. This is necessary for the mechanical properties. To accomplish this it is necessary to determine a forging strategy where there is an offset in between the bites to obtain a homogeneous strain distribution (figure 5.4).

The forging strategy is given by the forging simulation program ForgeBase. In figure 5.5 the effective-strain over the ingot length after the last pass is given. The points of maximal and minimal effective-strain for the coming microstructure analyses are shown as well.

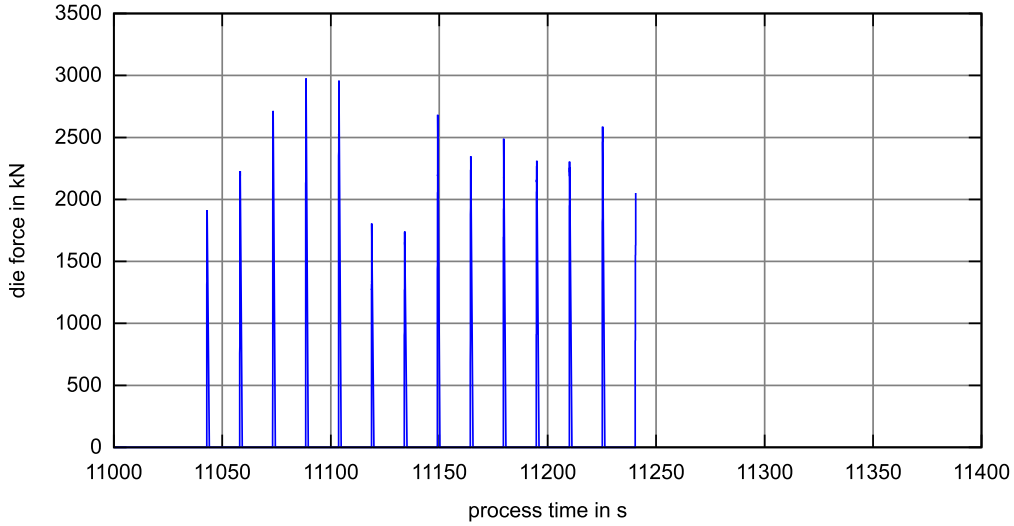

Figure 5.2: Forging forces for passes 3 and 4 as calculated by DEFORM3D

5.1.3 Temperature

Another crucial value for the quality of the forging process is the temperature progress. For a better formability and the activation of RX-/SRX-kinetics and grain growth the temperature should not drop under a certain level. Therefore a second heat after the second pass is necessary. For the temperature profile during the whole process for a point 100mm from the top of the ingot in the core see figure 5.7.

Furthermore, the temperature derivation in the core after the last pass is also of great interest, see figure 5.8. At the front of the ingot the temperature is a lot lower than in the rest of the ingot because of the heat flux over the front surface. Through the ingot the temperature is getting to a nearly constant level of ca. 1070°C. To the end of the forged ingot length the temperature rises again due to the greater not formed volume.

5.2 FORGE

FORGE, specifically FORGE3D, from Transvalor, primarily targets industrial users. It therefore resembles DEFORM in functionality and ease of use.

FORGE provides predefined so-called Presses which, based on a few values such as initial height, final height, number of blows etc., create a basic kinematic for an open die forging process. While this provides an easy way to get results for simple processes, it makes

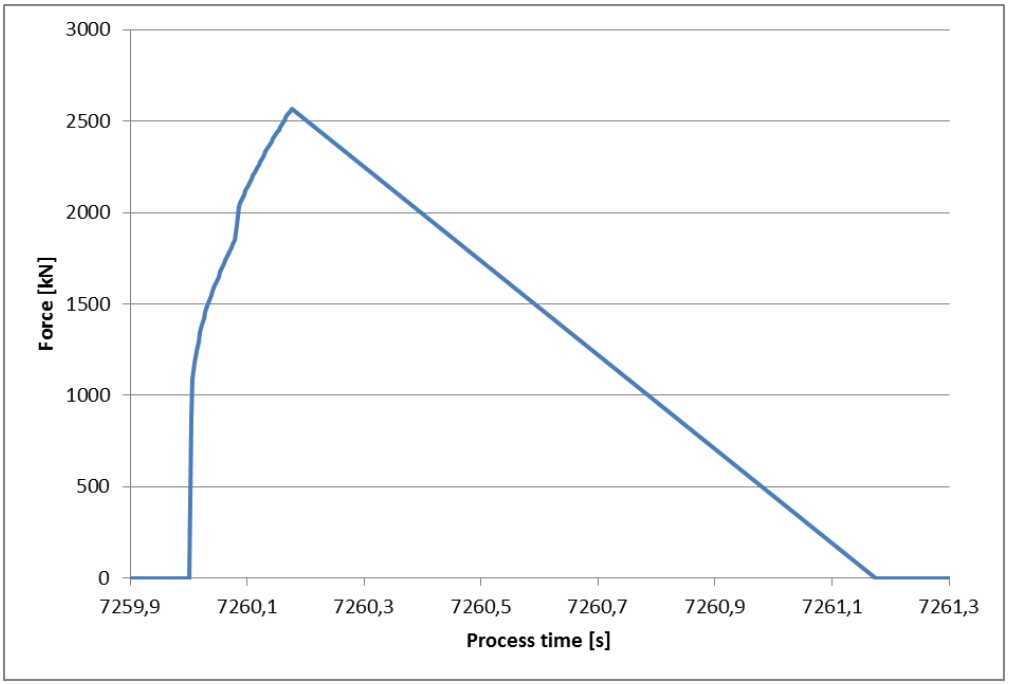

Figure 5.3: Forging force in the first blow as calculated by DEFORM3D

the setup of specific, more advanced processes rather difficult.

While it is possible to define custom presses and use these to model die kinematics, this function is hardly documented in freely available documents such as FORGE's online help system. This, however, leads to defining kinematics via basic linear and rotational movement operations in cases that do not meet the predefined standard processes. Especially in academic surroundings, where processes vary widely, the combination of undocumented functions to define presses and limited freedom to access and modify the process in-process makes adequate process definition difficult.

Similar to the definition of kinematics and movements is the adaption of the available material data for FORGE. While an extensive material data base is available, import of new material data is not well documented.

In FORGE, the process has been modelled symetrically with symmetry in the x-y and x-z planes. Apart from this, the model represents the real process in matters of die kinematics and work piece movement. That is, the die only moves in z direction while the work piece moves and rotates underneath it.

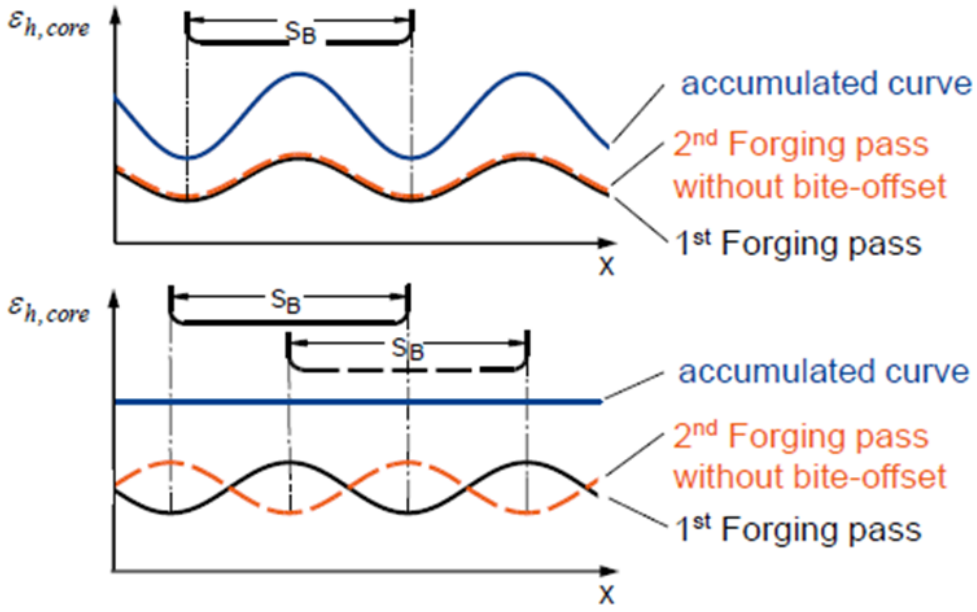

Figure 5.4: Influence of bite-offset on the equivalent strain in the core [Hir]

5.2.1 Forging Forces

The forging forces are shown in diagrams 5.10 and 5.11 for passes 1 and 2 and passes 3 and 4 respectively. As is expected, the force required for forging rises with each blow. In general, forging forces between 1.5MN and 2.0MN seem realistic, based on the calculations from Siebel's formula.

The diagram shows that a problem occurred in modelling pass 2. The peaks for the 2nd through 5th blow follow each other immediately, displaying a lack of waiting time in between. A closer examination of this will be seen below.

5.2.2 Strain

The effective strain in the core of the work piece after pass 4 is shown in diagram 5.12. A minimum value of 1.4 and a maximum value of 2.1 hint to a good forging of the core.

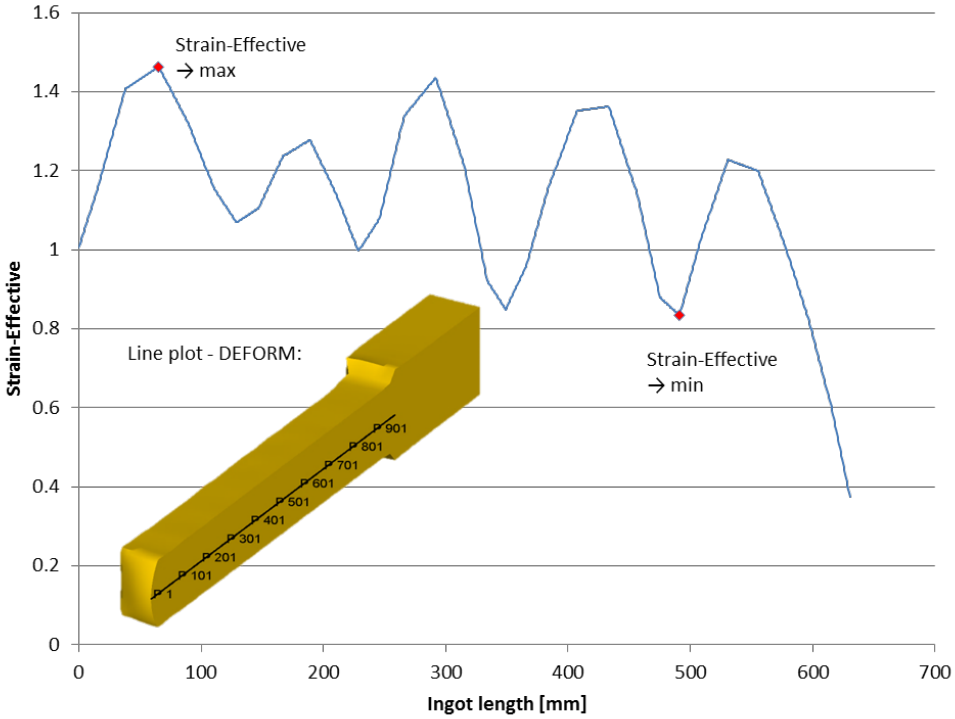

Figure 5.5: Effective strain in the core of the work piece after stroke 4 as calculated by DEFORM3D

5.2.3 Temperature

The temperature distribution in the core of the work piece after a cooling period of 120min is shown in diagram 5.13. Here, expectations are met as well by a low temperature at the head of the work piece, a fairly even distribution along its length and a rise in temperature at the end, which has not had any contact with the die.

Diagram 5.14 shows the temperature devolution of a node 100mm from the head of the work piece in its core. All stages of the process can clearly be seen here.

5.3 PEP/LARSTRAN

PEP/LARSTRAN is a combination of one pre- and postprocessing tool (PEP) and one solver (LARSTRAN). Both have been developed in an academic surrounding and accordingly provide more access to process variables during processing. On the other hand, a deeper understanding of FEM is necessary to use the system since values such

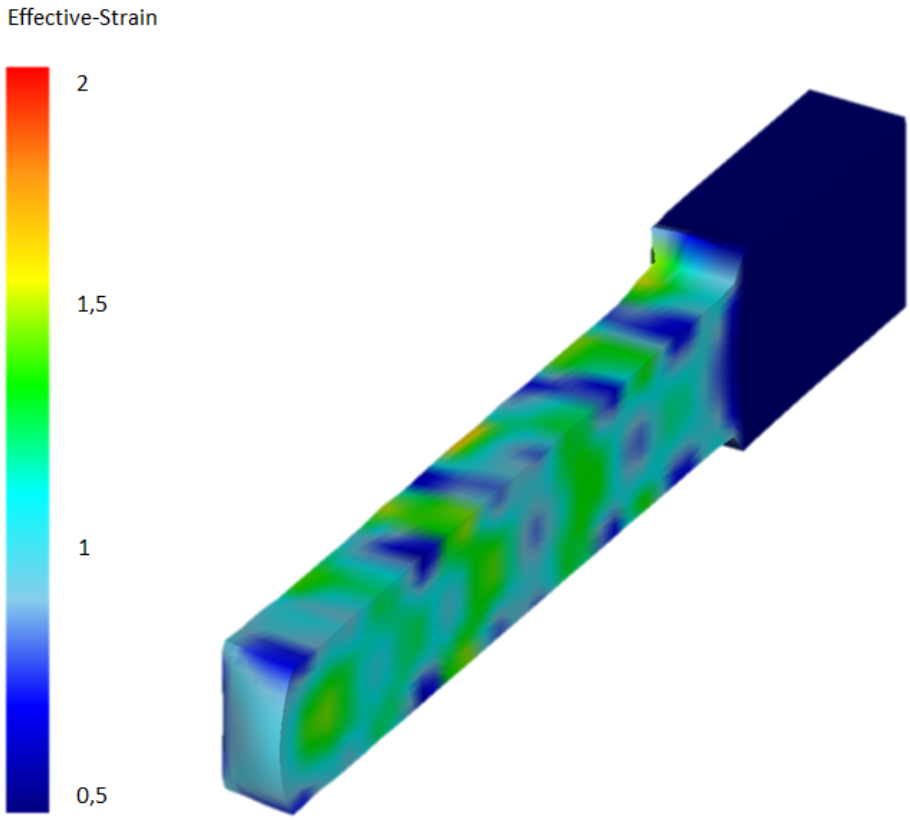

Figure 5.6: Effective strain in the work piece after stroke 4 as calculated by DEFORM3D

as time step length and mesh element edge length are not calculated automatically but rather have to be input by the user.

Kinematics control is done via a so-called model program. Here, die movements, changes in die speed and other process variables are defined to happen at a given time step. While other systems provide the concept of manipulators which exert a certain restore force on the die to prevent unrealistic work piece movement due to singular die contact, PEP/LARSTRAN does not allow for such possibilities. Similar functionality has been achieved by defining a fixing of the work piece based on the number of contact nodes, but certain differences can still arise.

PEP/LARSTRAN die kinematics are based exclusively on the movement of the dies instead of the work piece. Since the concept of model programs does not allow for the definition of die movement according to the current work piece situation, however, it

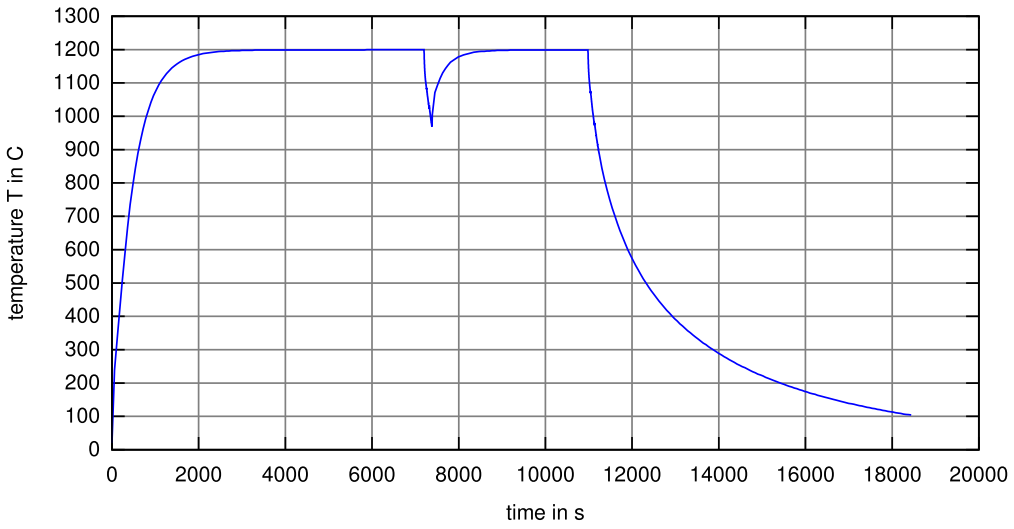

Figure 5.7: Temperature devolution of a point 100mm from the head in the core of the work piece as calculated by DEFORM3D

is not possible to even run one forging pass without stopping it and modifying the die movements. Moreover, the systems allows for only one ambient temperature, which means that each heating and cooling process and a combination of two forging passes have to be simulated separately and ambient temperature modified manually.

5.3.1 Forging Forces

The forging forces acting on the dies are shown in diagrams 5.15 and 5.16 for passes 1 and 2 and passes 3 and 4 respectively. Fitting the expectation, forces generally rise with an increasing number of blows due to strain hardening and material cooling. The last blow of each pass results in a smaller peak due to a shorter bite length in the last blow.

The forging force in the first blow of the second pass is considerably higher than that of the following blows. An explanation for this is an error in positioning the die for this blow, resulting in the die having contact with the work piece along its entire length, creating a larger contact area and, by that, a larger forging force.

5.3.2 Strain

The effective strain in the core of the work piece after pass 4 is shown in diagram 5.17. The values range between 0.4 and 1.4, which does not meet expectations. This could,

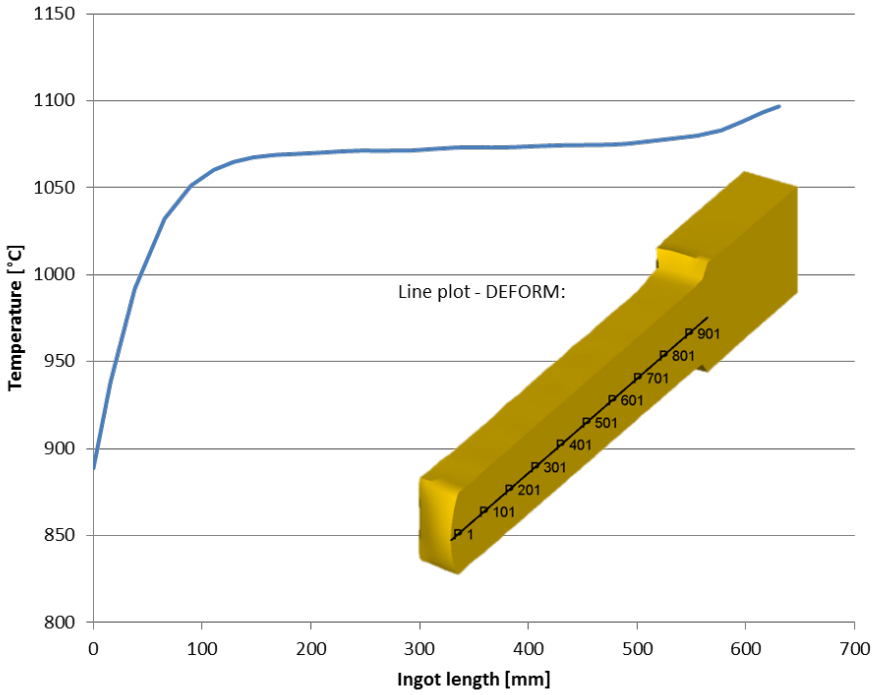

Figure 5.8: Temperature distribution along the core after cooling as calculated by DEFORM3D

however, be due to a mistake in modelling the second heating phase, which will be explained below.

5.3.3 Temperature

The temperature devolution of a node 100mm from the head of the work piece is shown in diagram 5.18. Here, it can be seen that the heating time for the second heating phase has not been reached, being only 360s instead of 3600s. Since tracking of nodal data is extremely strenuous and time-consuming in PEP's post-processing tool, only the first 100 steps of the third pass have been extracted, making up for only 17s.

Due to this difference in heating between the models, comparison of PEP/LARSTRAN's results of the temperature distribution at the end of the fourth pass does not seem useful.

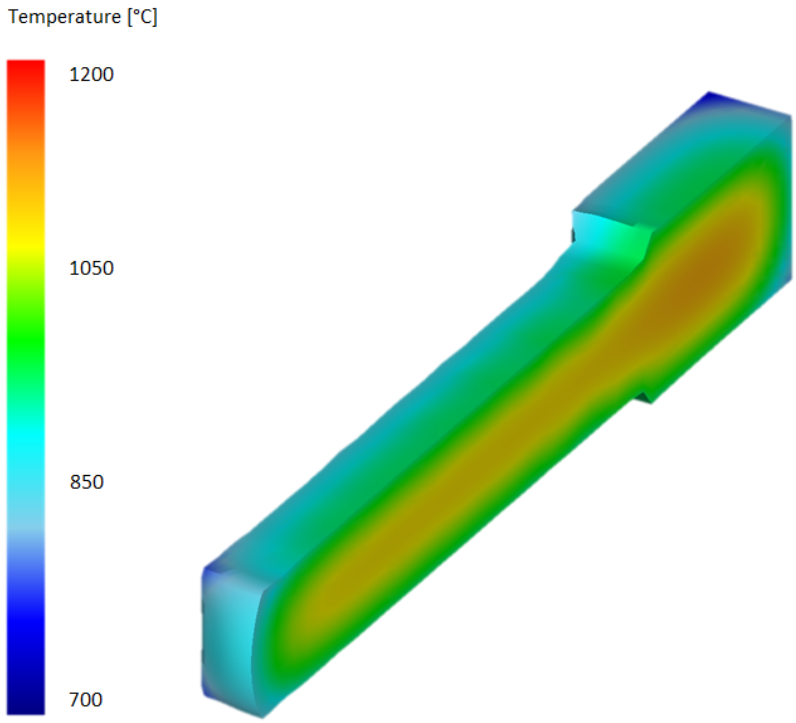

Figure 5.9: Temperature distribution along the core after cooling as calculated by DEFORM3D

5.4 Comparison of results

5.4.1 Forging forces

The resulting forging forces in all three systems are shown in diagram 5.19 for passes 1 and 2 and in diagram 5.20 for passes 3 and 4. One obvious difference is in the time between passes 1 and 2 and passes 3 and 4 respectively. While in DEFORM, no waiting period has been implemented, in FORGE and PEP/LARSTRAN, 45s have been introduced.

Another obvious difference is in the number of blows. While in DEFORM, passes 1 and 2 combine to 9 blows, in FORGE and PEP/LARSTRAN, there are 11 blows. Passes 3 and 4 show similar results. This can be explained by different lengthening of the work piece during forging, possibly stemming from different friction models or contact definitions.

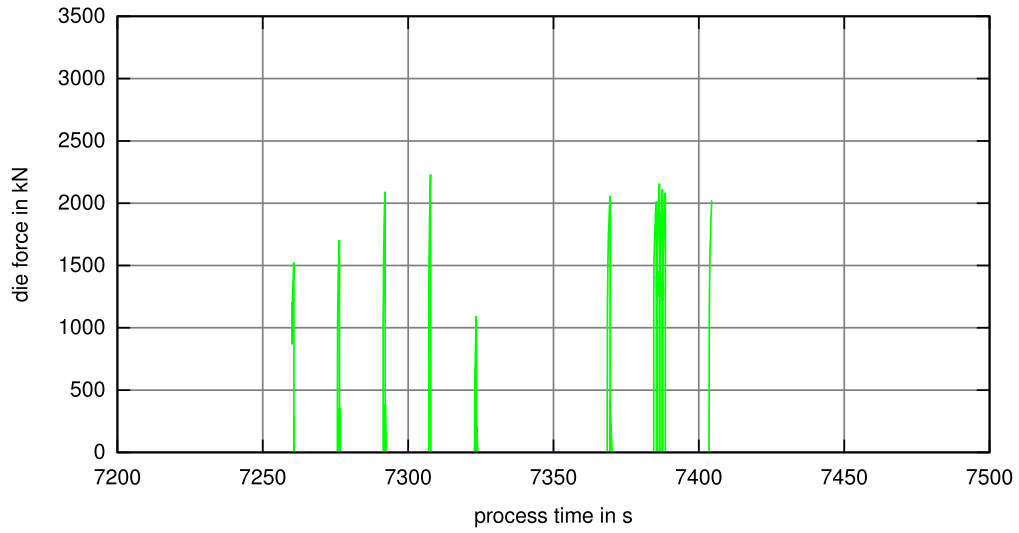

Figure 5.10: Forging forces for passes 1 and 2 as calculated by FORGE3D

Another reason, at least for PEP/LARSTRAN, could be that the work piece moves along its length during forging. Since PEP/LARSTRAN does not allow for in-process adaption to these movements, they may lead to shorter de-facto bite lengths and, finally, to more blows.

The forging forces are considerably higher in DEFORM than in FORGE and in PEP/LARSTRAN. While no explanation has been found for this, the consistency along the four passes hints to differences in material values or in the solvers.

5.4.2 Effective strain

The results for the effective strain in the core are compared in diagram 5.21. While the result from PEP/LARSTRAN should not be regarded due to the difference in heating time, it is obvious that the results from FORGE are considerably higher than those from DEFORM. This, again, might be due to differences in the use of the material data. However, the general shape of the strain distribution is fairly similar.

5.4.3 Temperature

The temperature distribution after the fourth pass is shown in diagram 5.22 for DEFORM and FORGE. Results from PEP/LARSTRAN are not shown due to the shorter heating period. Diagram 5.14 shows the temperature devolution of a node 100mm from

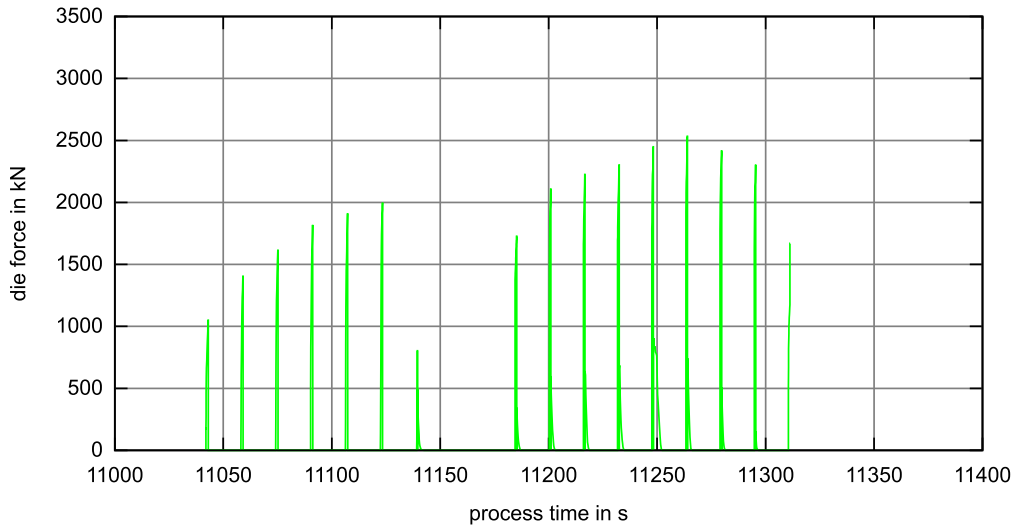

Figure 5.11: Forging forces for passes 3 and 4 as calculated by FORGE3D

the head of the work piece in its core.

Slower heating, a smaller drop in temperature and slower cooling that show in the results from FORGE would suggest a difference in either specific heat or heat conductivity. However, the same values have been used in both systems, so system-specific differences seem to be the cause for this difference. The results for PEP/LARSTRAN, where they can be compared to those from DEFORM and from FORGE, show a steeper rise in temperature during heating. During forging, the drop of the temperature is less steep when compared to the results from DEFORM and the drop is larger when compared to those from FORGE.

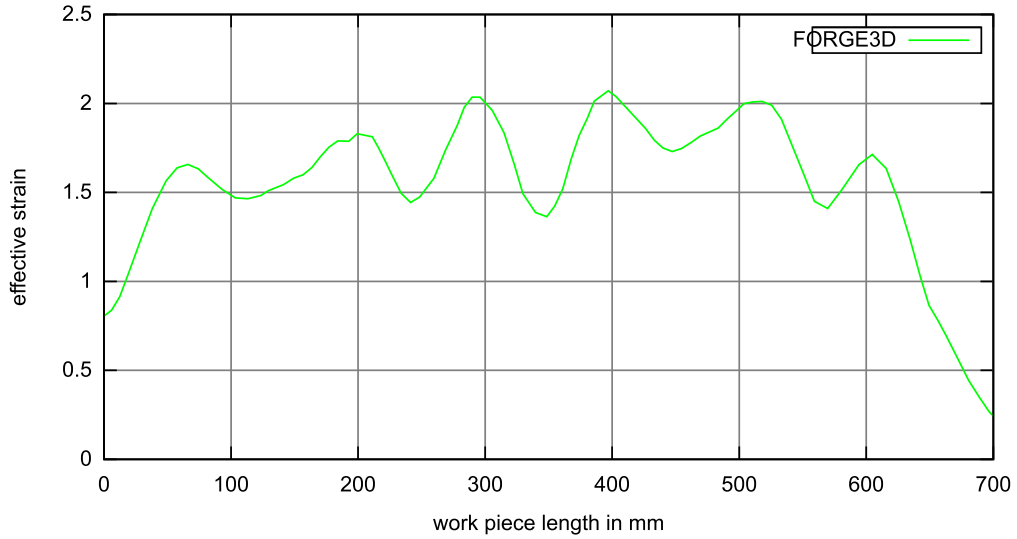

Figure 5.12: Effective strain in the core of the work piece after stroke 4 as calculated by FORGE3D

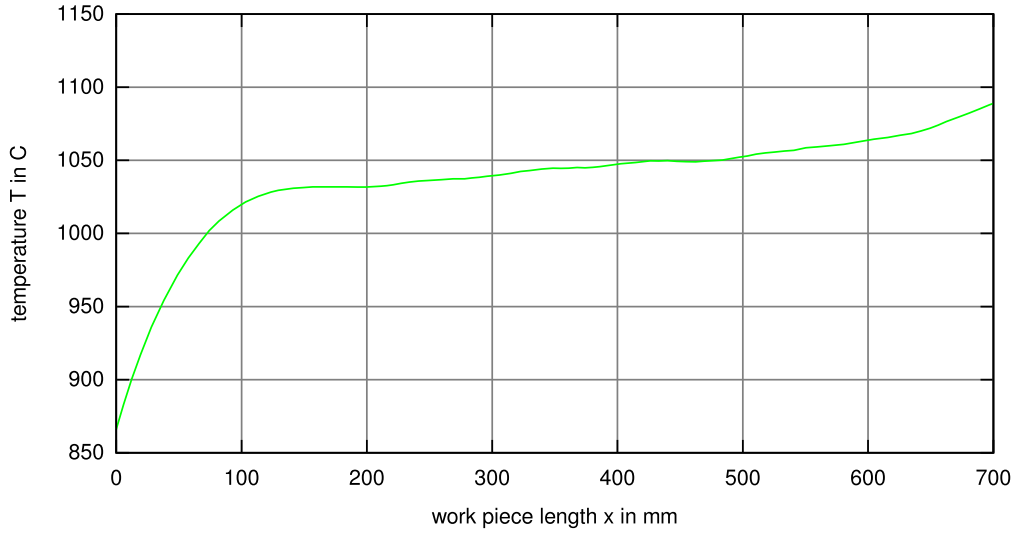

Figure 5.13: Temperature distribution along the core after cooling as calculated by FORGE3D

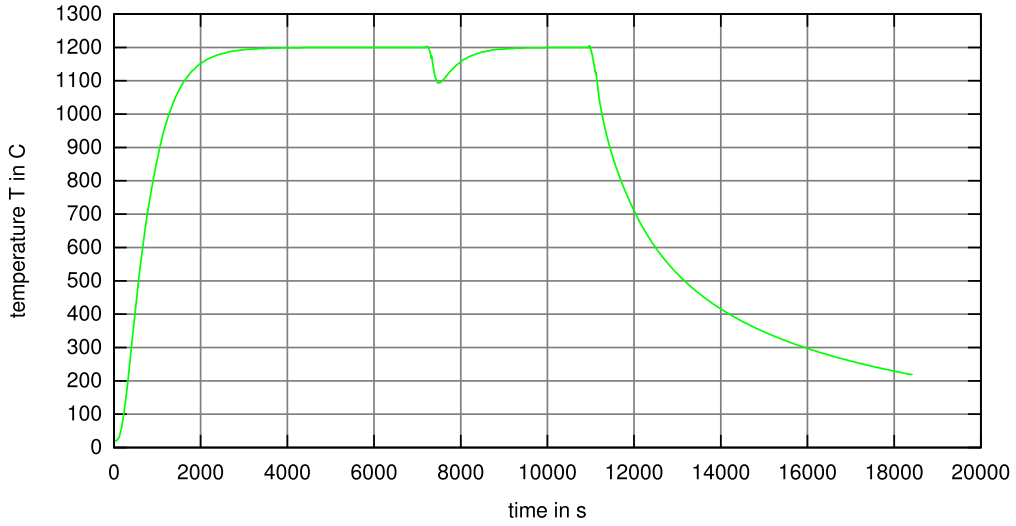

Figure 5.14: Temperature devolution of a point 100mm from the head in the core of the work piece as calculated by FORGE3D

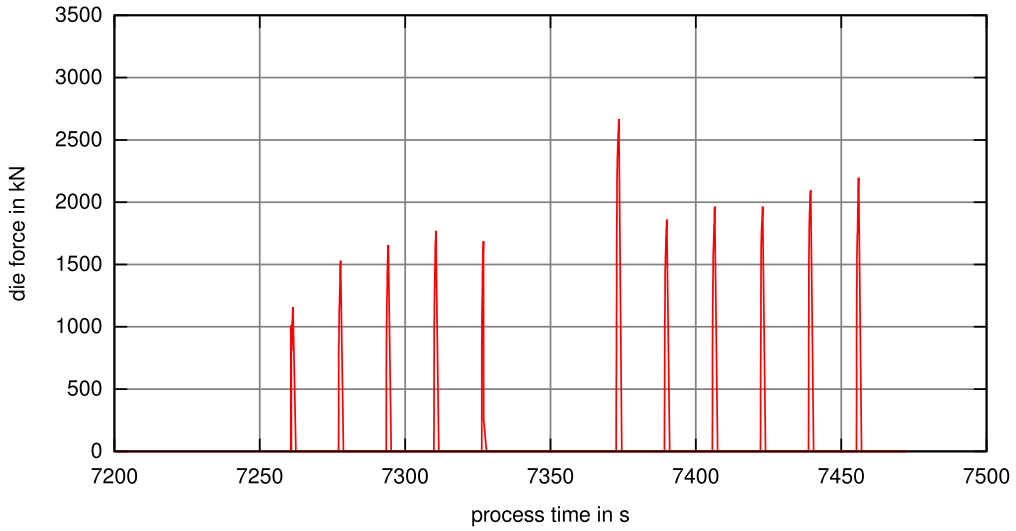

Figure 5.15: Forging forces for passes 1 and 2 as calculated by PEP/LARSTRAN

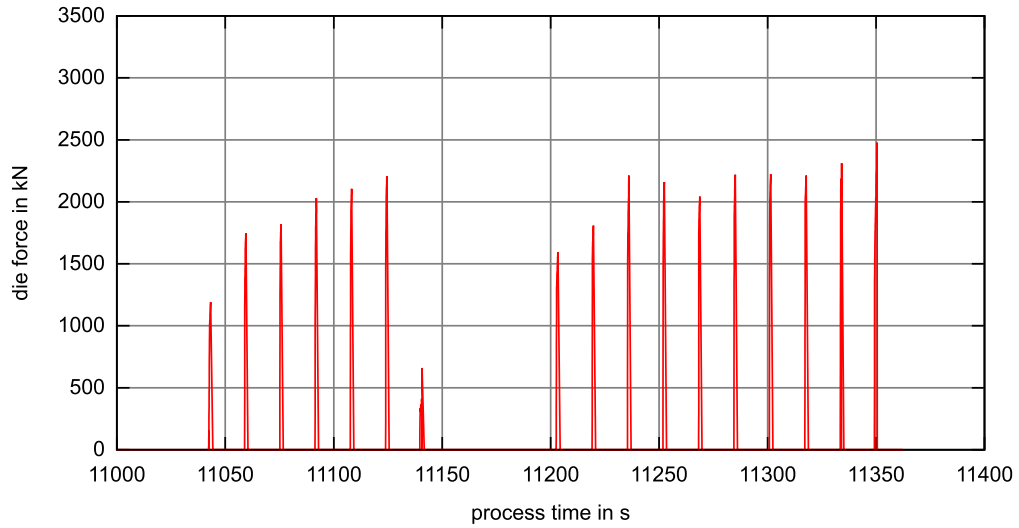

Figure 5.16: Forging forces for passes 3 and 4 as calculated by PEP/LARSTRAN

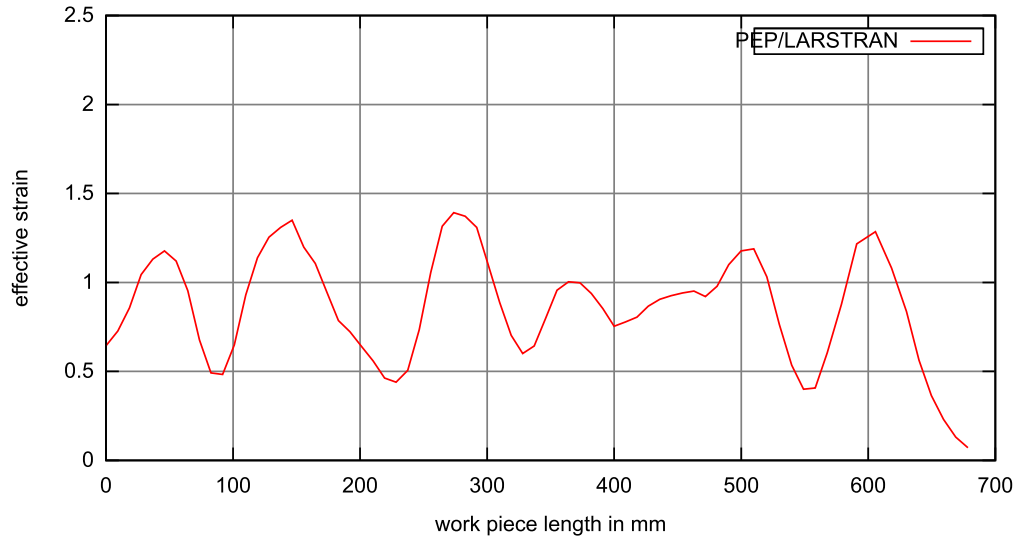

Figure 5.17: Effective strain in the core of the work piece after stroke 4 as calculated by PEP/LARSTRAN

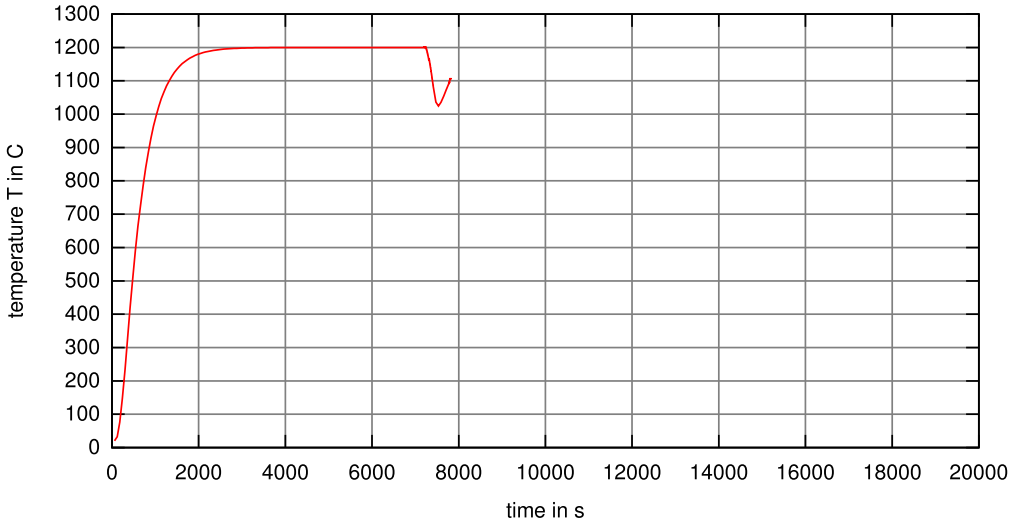

Figure 5.18: Temperature devolution of a point 100mm from the head in the core of the work piece as calculated by PEP/LARSTRAN

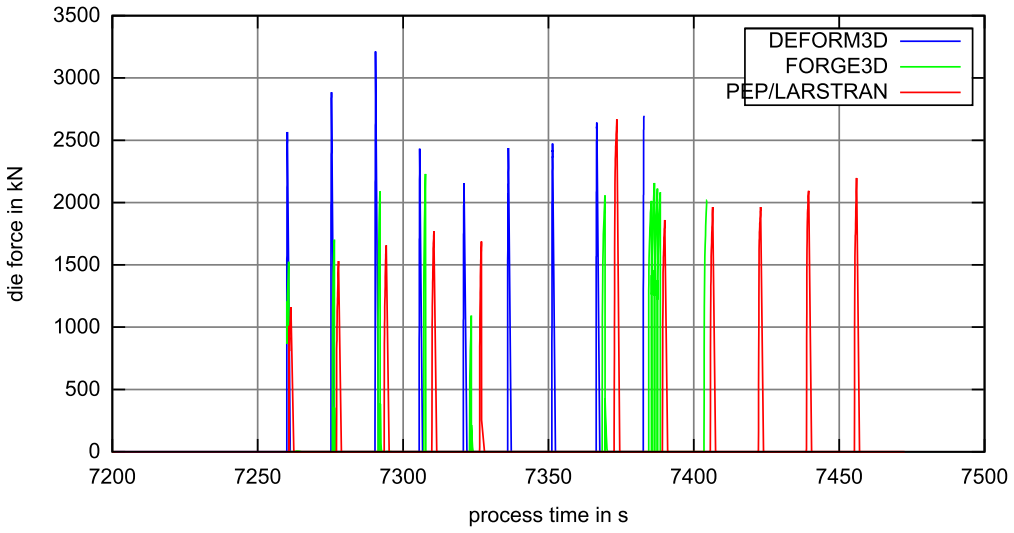

Figure 5.19: Comparison of forging forces for passes 1 and 2

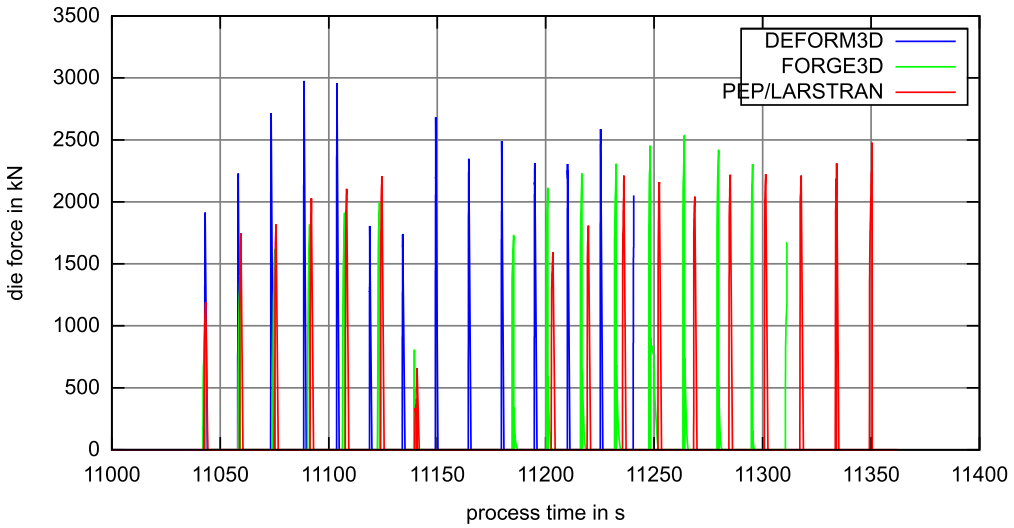

Figure 5.20: Comparison of forging forces for passes 3 and 4

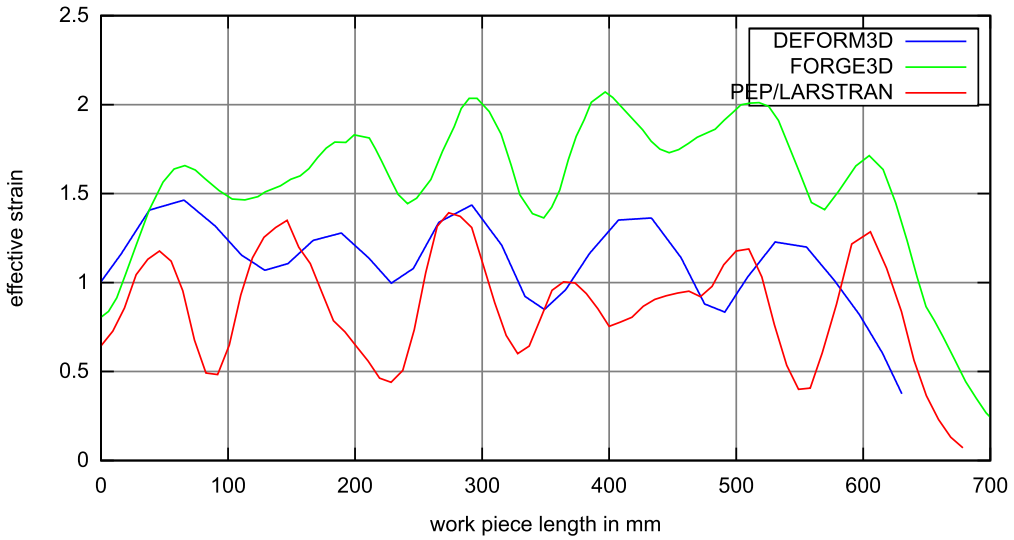

Figure 5.21: Comparison of the effective strain in the core of the work piece

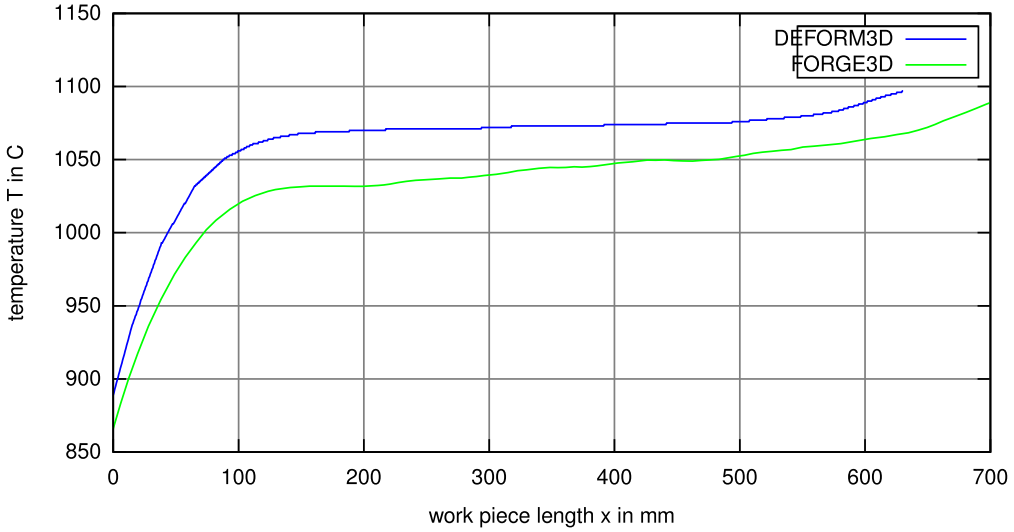

Figure 5.22: Comparison of the temperature distribution along the core after the fourth pass

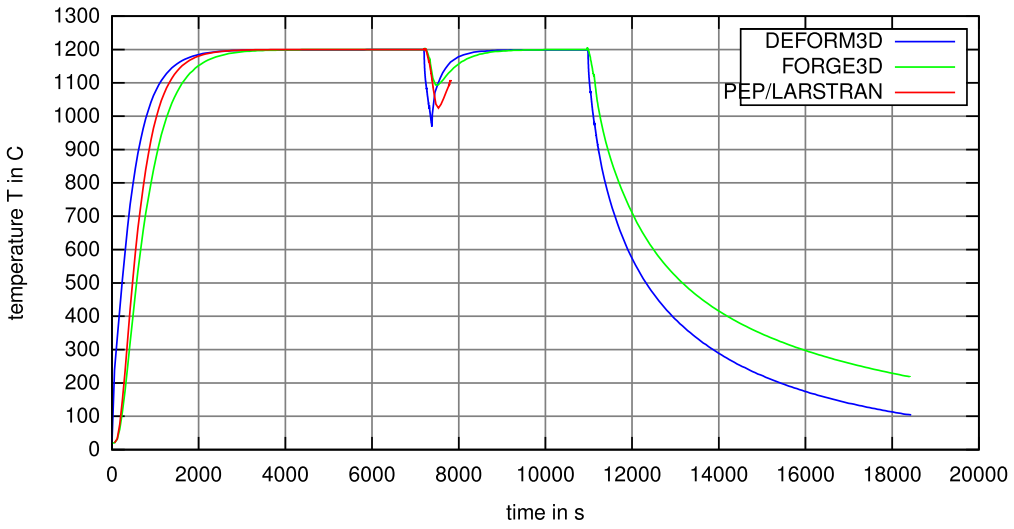

Figure 5.23: Comparison of the temperature devolution of a point 100mm from the head in the core of the work piece

6 Microstructure results

The microstructure development during the whole process is of great interest. Crucial values are the dynamic recrystallization (DRX) (during deformation), the static recrystallization (SRX), the recrystallized volume fraction (RX), which is the sum of DRX and SRX, and the average grain. For the mechanical properties of the product the microstructural development, the grain size in particular, is important to know. In this part the microstructure development during the different process stages will be discussed. To analyze the microstructure a subroutine is used which uses data from the point tracking in DEFORM for a point of maximal effective-strain and minimal effective strain as shown in figure 5.5.

The microstructure development for a point of maximal effective-strain is shown in figure 6.1. The initial grain size was set to $d = 70\mu m$. In the upper graph the temperature and strain development during the whole process is pictured. In the lower graph the DRX, SRX and RX volume fraction as well as the grain size is shown. It can be seen that the grain size increases during the first heat up to a saturation value (see figure 6.2) of $d \approx 85\mu m$. During the first and second pass (will be discussed in detail later) the grain size drops to a value of $d \approx 68\mu m$ due to DRX and SRX. In the second heat only SRX is taking place. The SRX kinetic is quite slow because of insufficient deformation before the second heat and is not completed at the end of the second heat so no grain growth is taking place. Afterwards, the third and fourth pass lead to a final grain size of $d \approx 65\mu m$.

The microstructure development during first and second pass is shown in figure 6.3. The dissipation during deformation can be seen in the upper graph. The temperature rises in maximum about $\Delta \approx 7°C$. During the passes DRX is taking place. After deformation SRX leads to a totally recrystallized volume fraction. After full recrystallization the DRX and SRX and thus the RX is set back to zero for the next deformation step. This is crucial for the multi pass design. In the second pass DRX and SRX are taking place again and lead again to a fully recrystallized volume fraction.

The microstructure development during pass 3 and 4 are shown in figure 6.4. In the third pass nearly no RX is taking place. However, in the fourth pass there is a leap in the SRX. This leap is the effect of a very small deformation as shown in figure 6.5. This is a problem of the used material model. Because of the small deformation the Zener-Holomon parameter is very small and this leads to a high DRX volume fraction. However the effect on the grain size is very small.

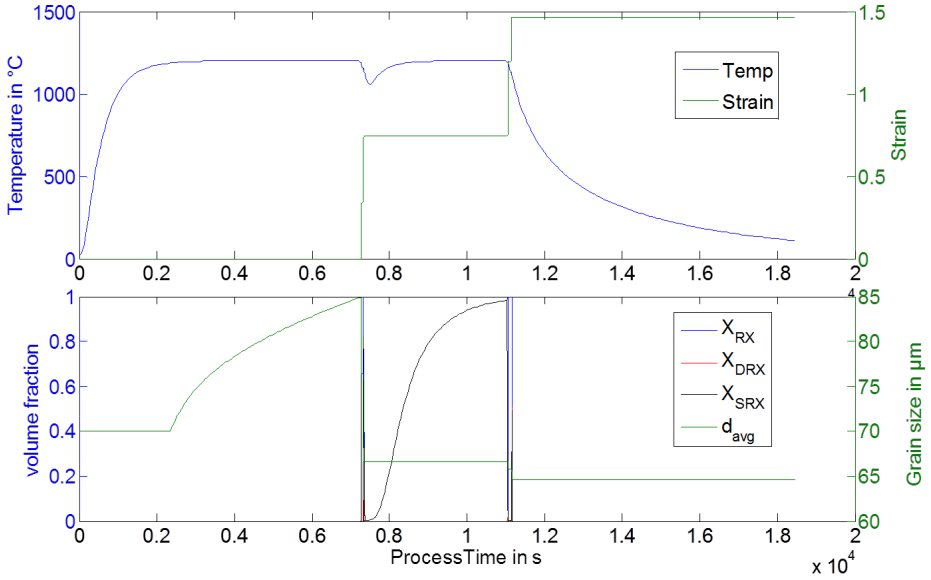

Figure 6.1: Microstructure development for max effective-strain during the process

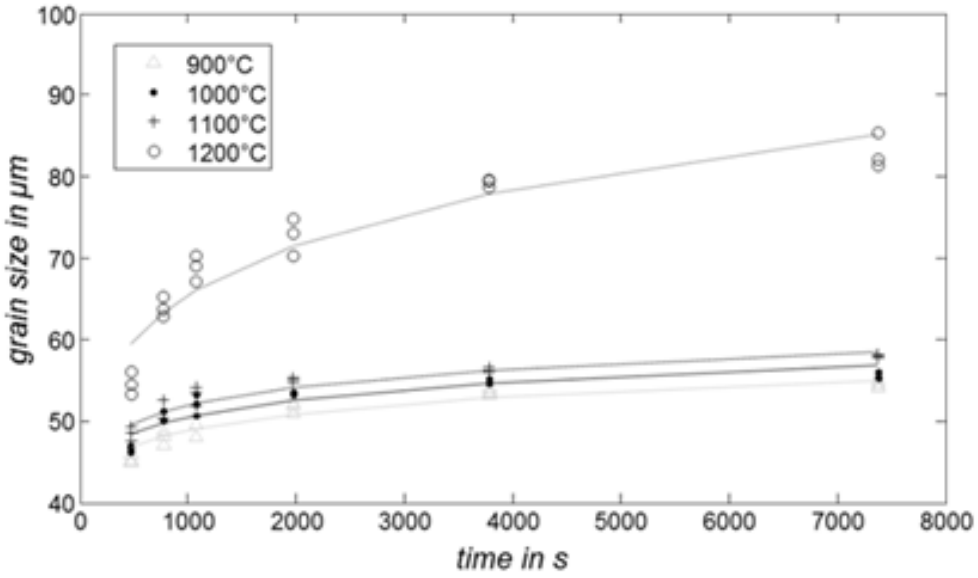

Figure 6.2: Modeled grain size [SHSH14]

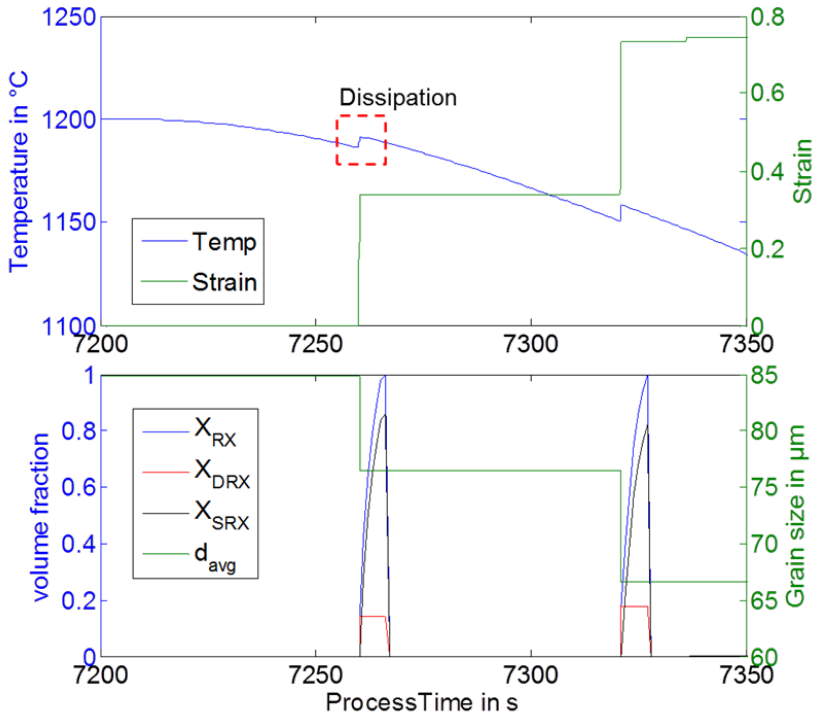

Figure 6.3: Microstructure development during pass 1 and 2

The DRX, SRX and therefore RX behavior in the point of minimal effective strain is similar to the one discussed bevore. However, the lower strain leads to a bigger grain size. After the last pass the grain size is about $d \approx 82\mu m$.

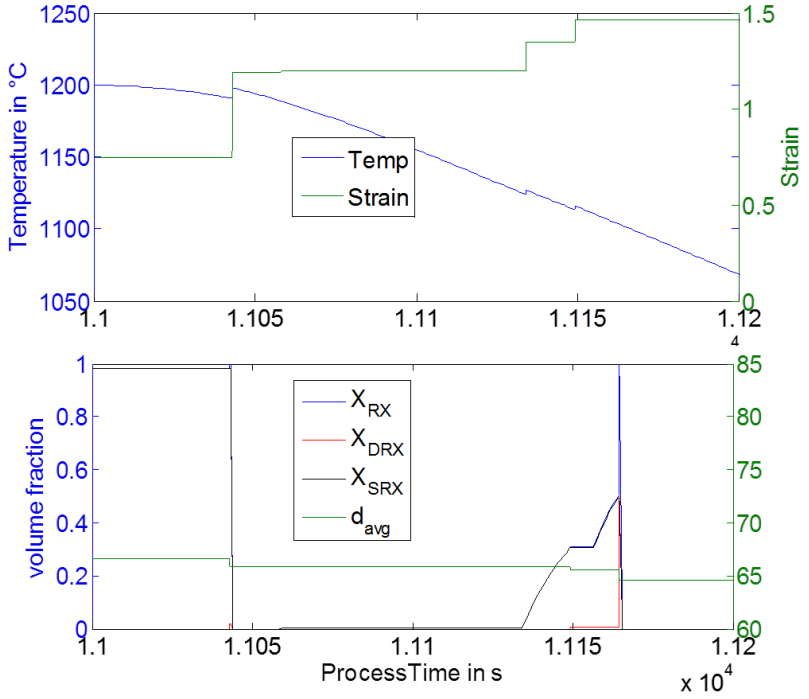

Figure 6.4: Microstructure development during pass 3 and 4

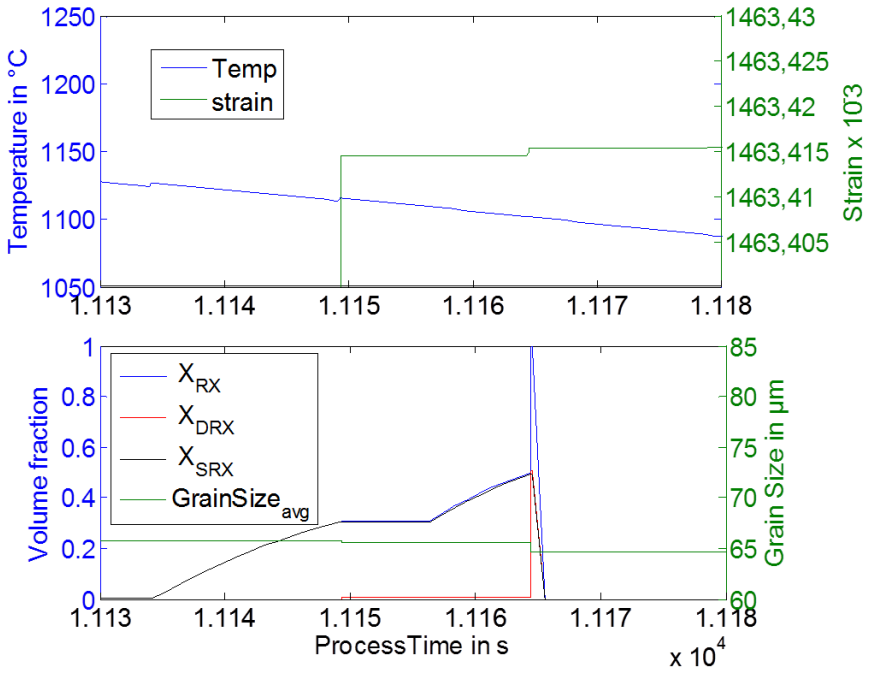

Figure 6.5: DRX leap during pass 4

7 Summary

It has been shown that the microstructural modelling of multi-pass open-die forging processes is possible. However, problems arise at small strain rates due to high resulting values for the dynamically recrystallized volume fraction. These, however, can be show to stem from a numerical effect at very small strain rates. This leads to SRX kinetics during the second heat that seem unrealistic. This leads to grain sizes that have to be evaluated critically.

The validation of the results from DEFORM has proven to be difficult. Differences in the approach of the various packages towards kinematics definition result in problems in recreating the process. However, where comparisons can be made, the systems still yield different results. This is especially obvious in the thermal modelling of the heating process, which is independent from die kinematics but still shows different results. Moreover, the resulting lengthening during the forging process differs between the used FEM packages, even leading to different numbers of blows needed to reach forging of the entire work piece.

In comparison, modelling in DEFORM using the cogging tool is a very handy way to setup an open-die forging model. Modelling open-die forging processes using FORGE is generally easy to do as well. However, more individual modelling leads to a sharp increase in the required effort. PEP/LARSTRAN, on the other hand, needs the user to have a deeper understanding of FEM as a concept and requires far more work in defining die kinematics.

8 Outlook

The results of microstucture modelling have shown that small strain rates result in large values for the dynamically recrystallized volume fraction. This effect is due to the limitations of using absolute thresholds for microstructural parameters. The models should be extended to give a more dynamic model which allows a bigger range of these paramenters.

Furthermore, a systematic approach to the comparison of various FEM packages with each other and with reality should involve, as a first step, the research of the capabilities of the involved packages and the development of an according model process. Also, an even more detailed process model should be set up, using the same time increments, mesh, boundary conditions etc.

Lastly, a validation of the results in a real process is necessary. This includes a validation of both the microstructural model with grain sizes measured during the process and the process parameters such as die forces and material temperature development.

List of Figures

References

[ARP08] A., Deghan-Manshadi ; R., Barnett M. ; P.D., Hodgson: Hot Deformation and Recrytallization of Austenitic Stainless Steel: Part 1. Dynamic Recrystallization. In: *The Minerals, Metals & Materials Society and ASM International* (2008)

[CH44] C., Zener ; H., Hollomon J.: Effect of Strain Rate Upon Plastic Flow of Steel. In: *Journal of Applied Physics Vol.15* (1944)

[DB07] Doege, Eckart ; Berens, Bernd-Arno: *Handbuch Umformtechnik*. 1. Berlin; Heidelberg; New York : Springer, 2007. – ISBN 978–3–540–23441–8

[DEF14] DEFORM: *DEFORM-3D*. http://www.deform.com/wp-content/uploads/2011/03/3D_brochure.pdf, 2014. – [Online; abgerufen am 14.03.2014]

[DHK+11] Dahme, Michael ; Hirschvogel, Manfred ; Kettner, Peter ; Landgrebe, Dirk ; Pischel, Walter ; Raedt, Hans-Willi ; Ruile, Christoph ; Schleich, Michael ; Wondrak, Jürgen: *Massivumgeformte Komponenten - Forged Components*. Landsberg am Lech : Hirschvogel Automotive Group, 2011

[Ede08] Edelstahlwerke, Deutsche: *1.4301 X5CrNi18-10*. http://www.dew-stahl.com/fileadmin/files/dew-stahl.com/documents/Publikationen/Werkstoffdatenblaetter/RSH/1.4301_de.pdf, 2008. – [Online; abgerufen am 31.01.2014]

[Got07] Gottstein, Prof. Dr. G.: *Physikalsiche Grundlagen der Materialkunde*. 3. Aachen : Springer, 2007. – ISBN 978–3–540–71104–9

[Hir] Hirt, Gerhard: *Vorlesungsskript – Grundlagen und Lösungsverfahren der Umformtechnik*

[Kar94] Karhausen, K. F.: *Integrierte Prozeß- und Gefügesimulation bei der Warmumformung*, RWTH Aachen, Diss., 1994

[Loh10] Lohmar, Johannes: *Modular Framework for the simulation of metal-physical events during hot working*, RWTH Aachen, Masterarbeit, 2010

[met14] metallograf.de, Werkstoffkartei: *1.4301 X5CrNi18-10*. http://metallograf.de/, 2014. – [Online; abgerufen am 31.01.2014]

[MJJ03] M., El W. ; J.M., Cabrera ; J.M., Prado: Hot working of two AISI 304 steels: a comparative study. In: *Materials Science and Engineering* (2003)

[SHSH14] Schwich, Gideon ; Henke, THomas ; Seitz, Joachim ; Hirt, Gerhard: Prediction of microstructure and resulting rolling forces by application of a material model in a hot ring rolling process. In: *Metalforming* (2014)